Journal of Magnetic Resonance **156,** 72–78 (2002)
doi:10.1006/jmre.2002.2543

Multiple Spin Echoes in Heterogeneous Systems: Physical Origins of the Observed Dips

F. M. Alessandri,* S. Capuani,*,† and B. Maraviglia*,†,[1]

*Dipartimento di Fisica Università di Roma "La Sapienza," 00185 Rome, Italy; and †Istituto Nazionale Fisica della Materia (INFM), UdR Roma1 and Enrico Fermi Center, Rome, Italy

Received September 24, 2001; revised April 4, 2002

Dipolar interactions in liquids have recently offered a new challenge to investigate porous media by exploiting intermolecular quantum coherences, which are obtained through a simple two-pulse sequence (90°–τ–120°). This sequence, in the presence of an external gradient (G), refocuses a train of echoes at multiple integer values of time τ. The first and second echo amplitudes are acquired for heterogeneous systems such as porous media at different time values (τ). In our first experiments on bovine bone samples we have observed unpredicted dips on the second echo time behavior. We argue that a strict relation occurs between the average pore dimensions and the dips time position through the correlation distance $d = \pi/\gamma G\tau$ (defined as half a cycle of the magnetization helix, which originates in the presence of an external gradient). Although the experimental results have revealed an exceptional connection between the porous structure and the correlation distance, no physical explanation was so far provided. In this paper we propose a possible physical cause of the observed phenomenon. In addition we report an accurate analysis of new experiments performed on glass beads phantoms, which confirms our conclusions.

Key Words: **long range dipolar interactions; MSE (multiple spin echoes); porous media; demagnetizing field; double quantum coherence.**

INTRODUCTION

A porous medium is a highly inhomogeneous system that does not usually present particular internal symmetries. Structural information by NMR is generally achieved through relaxation time studies and diffusion coefficient D measurements.

It was recently recognized that residual long range dipolar coupling provides a novel contrast mechanism to study heterogeneity in liquid systems (*1–3*) and tissues (*4–9*). A simple two-pulse sequence (90°–τ–120°) together with a constant linear magnetic gradient G are used to produce a train of echoes (*10, 11*). In the presence of an external magnetic gradient G the long range term of the dipolar demagnetizing field B_d acts over a correlation distance

$$d = \frac{\pi}{\gamma G\tau} \qquad [1]$$

(which is half a cycle of the magnetization helix) and depends only on the local magnetization. The second echo amplitude was found to depend on the sample heterogeneity over the distance d (*3*). By changing the strength and duration of the external gradient the pitch of the spatially modulated magnetization varies, thus probing the sample heterogeneity over a specific length scale. In our recent papers (*12, 13*) we observed particular and unpredicted dips, which appeared on the second echo amplitude behavior, when the time τ varied. These dips seemed to occur every time the correlation distance d became comparable to the average pore size of a porous system.

In our works (*12, 13*) the structure-sensitive nature of the multiple spin echoes (MSE) method was employed to probe the pore size distribution in bovine bone samples. The bone microstructural architecture can be considered a very complex porous medium made of thin trabeculae, characterized by length scales ranging from a few up to ~900 μm (*14*). There we demonstrated that the theoretical predicted behavior of Eq. [6] presents large discrepancies with the experimental results in such heterogeneous and highly anisotropic systems. It was also observed that the bone trabecular linear dimensions and the correlation distance d match excellently when d (Eq. [1]) is computed in correspondence of the time τ values for which the signal minima appear.

We extended our MSE technique study to other porous media, such as porous stones (*16*). We chose highly heterogeneous systems such as sedimentary stones both in order to confirm the discrepancies with theory found in bovine bone samples and, of course, for the potential important information that MSE could provide for such materials. Indeed sedimentary stones, such as travertine, are composed by a calcium carbonate matrix, characterized by low porosity and low paramagnetic impurities concentration. The pore size dimensions range from a few tens of nanometers to some hundreds of micrometers. Again the

[1] To whom correspondence should be addressed.

1090-7807/02 $35.00

average pore size and the correlation distance, obtained by the time position corresponding to the dips, match well.

The need for a more detailed analysis of these unexpected results brought us to plan some experiments on phantoms whose pore size distribution was well defined. A systematic comparison between the results we obtained on these standards and on the homogeneous samples then allowed a better understanding of the physical origins of the dips which we discovered on the second echo envelope. Thus the main goal of this paper is to physically explain the origin of the dips and the relation between the dips' position and the correlation distance d.

BACKGROUND THEORY

The effects of dipolar interaction, between nuclear spins, in liquids are generally neglected. This assumption is true because of the angular dependence of the dipolar interactions Hamiltonian

$$\hat{H}_D = \frac{\mu_0}{4\pi} \sum_{i \neq j} \left(\frac{\hat{\mu}_i \cdot \hat{\mu}_j}{r_{ij}^3} - 3 \frac{(\hat{\mu}_i \cdot \mathbf{r}_{ij}^3) \cdot (\hat{\mu}_j \cdot \mathbf{r}_{ij}^3)}{r_{ij}^5} \right),$$

where $\hat{\mu}_i = \gamma \hbar \hat{I}_i$, with $i = 1 \ldots N$, are the magnetic moment operators for a N-spins homonuclear system. Short range interactions are active when the distance between spins is smaller than the diffusion length, $d < l_D \approx \sqrt{D \cdot t} \approx 10\ \mu$m, where t is the NMR time scale. In this case dipolar interactions are efficiently averaged to zero by diffusion:

$$\langle 1 - 3 \cdot \cos^2 \theta \rangle_\Omega = 0.$$

However, when the distance between the interacting spins increases, diffusion is unable to average the dipolar interaction to zero efficiently. At any rate, if the magnetization is spatially isotropic, the dipolar interactions are geometrically averaged to zero over the sample by symmetry, also at long distances.

When the magnetization isotropy is broken, by applying an external magnetic gradient G along the direction $\hat{s}$, the long range dipolar interaction term reappears and the transverse magnetization forms a spatial helix (Fig. 1) whose pitch is defined as

$$p = \frac{2\pi}{\gamma G \tau}, \qquad [2]$$

where G is the external gradient intensity and τ the duration of the gradient. It is worth pointing out that a system can be considered homogeneous when the helical pitch is small compared to the pore linear dimensions.

Within the classical formalism the expression, which accounts for the long range dipolar interaction, is called the demagnetizing field and it is described within the mean field approximation by

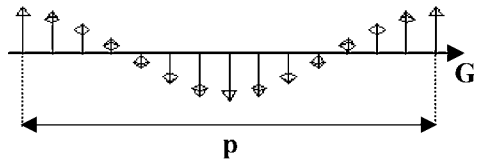

FIG. 1. When an external gradient is applied, the transverse magnetization forms a spatial helix with pitch p (Eq. [2]).

$$B_d(\mathbf{r}) = \frac{\mu_0}{8\pi} \int_V \frac{1 - 3 \cdot \cos^2 \theta}{|\mathbf{r} - \mathbf{r}'|^3} \cdot (3 \cdot M_z(\mathbf{r}') \cdot \hat{z} - \mathbf{M}(\mathbf{r}'))\, d^3 r', \quad [3]$$

where θ is the angle between the internuclear vector $\mathbf{r} - \mathbf{r}'$ and the static field $\boldsymbol{B}_0$.

Deville *et al.* (*15*) recognized a convolution product in the demagnetizing field. Indeed, by considering that the only spatial dependence is along the external gradient direction $\hat{s}$, the Fourier transform of the demagnetizing field, first forward and then backward, gives the simpler expression

$$\mathbf{B}_d(s) = \beta(\hat{s}) \cdot \left(M_z(s) \cdot \hat{z} - \frac{\mathbf{M}(s)}{3} \right), \qquad [4]$$

where β is defined as

$$\beta(\hat{s}) = \frac{\mu_0}{2} (3(\hat{s} \cdot \hat{z})^2 - 1).$$

The modified Bloch equation, if the dipolar interactions are included, becomes nonlinear and can be solved for the MSE sequence shown in Fig. 2.

The solution for homogeneous systems can be achieved writing the transverse magnetization as a Fourier series (*10, 11*). The nth harmonic is then refocused at a time $n\tau$ after the second RF pulse, as a consequence of the dipolar interactions on spins separated by the correlation distance, giving the nth echo. In particular the first (A_1) and second (A_2) echo amplitude are

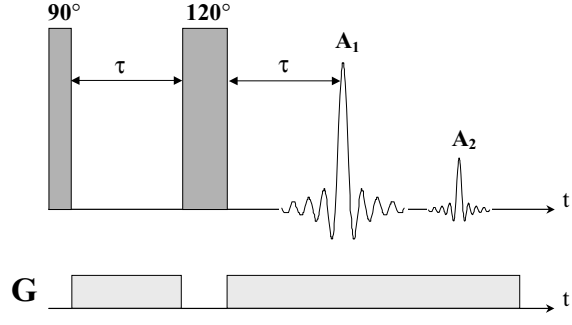

FIG. 2. Two pulse sequence implemented to generate multiple spin echoes. Intermolecular multiple quantum coherences evolve during the interpulse time τ and are detected after being transformed into observable magnetization.

described as

$$|A_1(\tau)| = M_0 \cdot e^{-\frac{2}{3}\cdot D^*} \cdot e^{\frac{2\cdot\tau}{(T_2^*)'}} \quad [5]$$

$$|A_2(\tau)| = \frac{\gamma\beta \cdot M_0^2}{2} \cdot \frac{e^{-\frac{7}{3}\cdot D^*}}{\sqrt{D^*}} \cdot \tau \cdot \sqrt{\pi} \cdot erf(\sqrt{D^*}) \cdot e^{-\frac{4\cdot\tau}{(T_2^*)'}}, \quad [6]$$

where $erf(\sqrt{D^*})$is the error function, $D^* = D \cdot (\gamma G)^2 \cdot \tau^3$, and $(T_2^*)'$ includes both double- and single-quantum T_2^* effects (*17*). The first and second echo amplitude analytical behavior as a function of time τ is experimentally verified for homogeneous systems.

As demonstrated in many well-known papers (*3, 4*) the double quantum signal that is refocused on the second echo comes primarily from spins whose distance is just d (i.e., the correlation distance).

METHODS AND MATERIAL

The sensitivity of the MSE sequence is reduced compared to conventional single quantum techniques and a large number of signal acquisitions is required to achieve a sufficient signal to noise ratio (S/N). The number of signal averages used in our experiments is generally around 64 with a repetition time of 10 s between each acquisition. The RF pulses duration used in the MSE sequence (Fig. 2) was set to 50 and to 66.7 μs for the 90° and 120° pulses, respectively.

The phantoms were made of hollow ellipsoidal plastic holders of 45 × 30 mm, filled either with 0.5-mm or with 1-mm radius glass (Pyrex glass) beads. To improve packing, the beads were laid one layer at a time. Every time a layer had been covered, the spheres were let to settle with short vibration. The phantoms were finally filled with distilled water. We made the assumption that the beads were displaced in a regular hexagonal lattice. Thus the interstitial spaces between the close-packed spheres form a structure of connected pores and their linear dimensions l were estimated for both samples to be comparable to the radius length: $l(R = 0.5\text{ mm}) = 0.53$ mm and $l(R = 1\text{ mm}) = 1.03$ mm.

All NMR experiments were performed on a 7-T Bruker Biospec (15-cm bore) system equipped with maximum magnetic field gradients intensity of 46 mT/m with 300-μs rise time. RF pulse transmission and signal detection were performed with a ^{1}H Alderman & Grant probe (6-cm internal diameter).

RESULTS AND DISCUSSION

A considerable help to understand the physical origins of the observed dips comes from an accurate analysis of the data obtained from the packed beads samples. In Fig. 3 the second echo amplitudes are compared respectively for a free water sample (Fig. 3a, spherical sample of 3-cm diameter, filled with distilled water) and for the sample with the 0.5-mm radius beads (Fig. 3b), both acquired with a gradient intensity of $G = 19.7$ mT/m applied along the $\hat{x}$ direction.

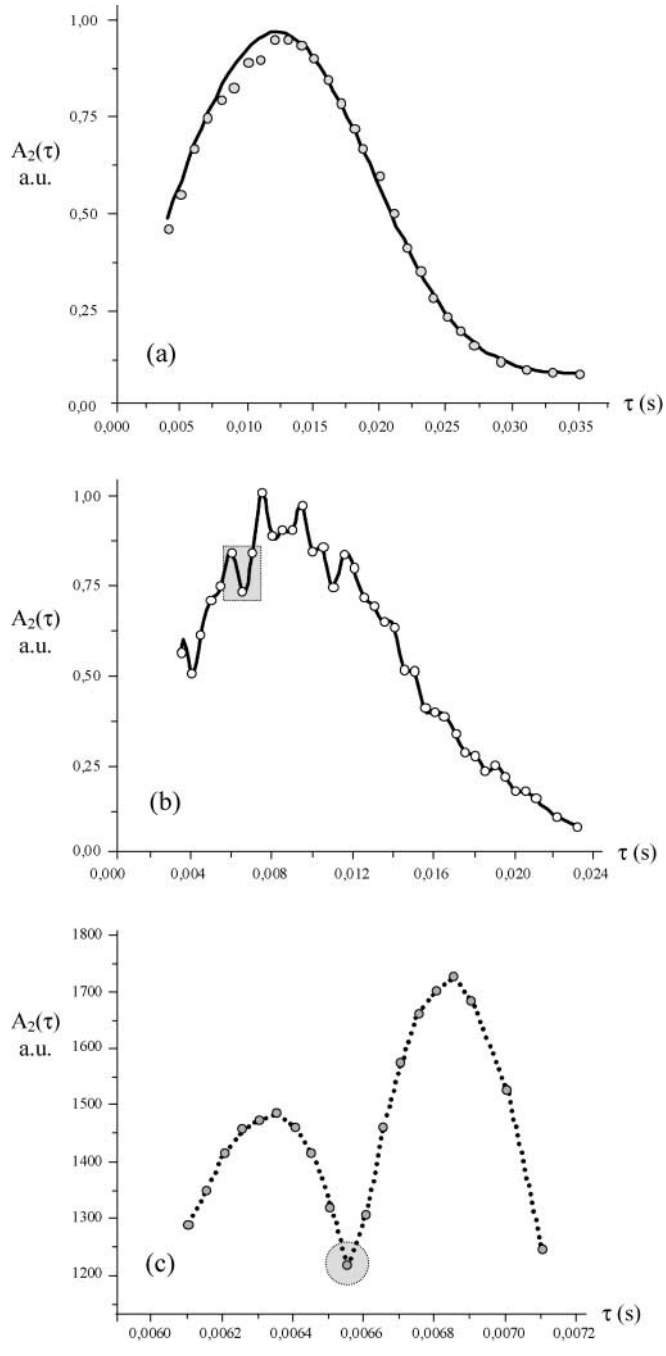

FIG. 3. Comparison between the second echo amplitudes as a function of time τ, (a) for the free water sample and (b) for the sample with 0.5-mm radius beads. In (c) the intensified acquisition is reported for the region marked in (b). The acquisition parameters are the same for both samples: Averages = 64, $G = 19.7$ mT/m applied along the $\hat{x}$ direction. The correlation distance computed for the minimum shown in (c) is equal to (0.57 ± 0.01) mm in good agreement with the estimated linear dimension of the pore by geometrical considerations.

The best fit to the free water sample obtained by Eq. [6] (solid line in Fig. 3a) well matches the experimental data behavior. The $(T_2^*)'$ relaxation time and the diffusion coefficient values, obtained as fit parameters, are equal to (1.40 ± 0.10) s

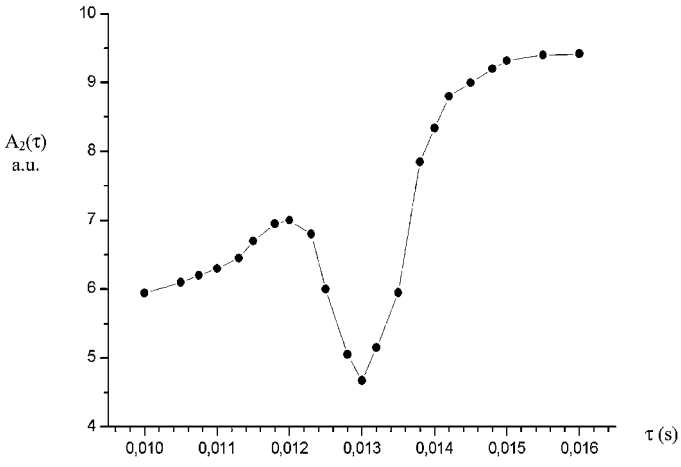

FIG. 4. Second echo amplitudes for a sample made of 1-mm radius beads. Averages = 64, $G = 4.8$ mT/m applied along the $\hat{x}$ direction. The correlation distance computed for the minimum shown is equal to (1.18 ± 0.01) mm.

and $(2.35 \pm 0.02)10^{-9}$ m^2/s, respectively. The second echo amplitudes acquired (by varying the time τ) for the heterogeneous sample exhibits a very irregular behavior characterized by periodic signal dips. The partial destruction of the acquired signal is not simply a noise effect—repeated measurements have generated the same results. This irregular behavior is in fact caused by the heterogeneous structure of the system and can be verified in Fig. 3c, where the magnification and intensification of a small portion of Fig. 3b confirms the continuity of the function behavior. The correlation distance $2\pi d$ computed for the minimum shown in Fig. 3c is equal to (0.57 ± 0.01) mm.

In Fig. 4 the second echo amplitudes for a sample made with 1-mm radius beads acquired with a gradient intensity of $G = 4.8$ mT/m are reported to confirm the strict correlation between the time dependence of the second echo amplitudes and the pore sizes. As a matter of fact also in this case, the correlation distance $2\pi d$ computed for the minimum shown in Fig. 4, that result equal to (1.18 ± 0.01) mm, is about the average pore diameter previously estimated by geometrical considerations.

In Fig. 5a the amplitude $A_1(\tau)$ of the first echo as a function of τ, corresponding to the data of $A_2(\tau)$ in Fig. 3b, is shown. In Fig. 5b we report the $A_1(\tau)$ data relative to the acquisition of $A_2(\tau)$ in Fig. 3c. In this case, no dips appear as a direct consequence of the different nature of the signals acquired on the first and second echo amplitude. As a matter of fact, the second echo amplitude originates from double quantum coherences established during the first evolution time between the two pulses and selected through the correlation distance d. The first echo amplitude instead is due to single quantum transition, as the theoretical expression (Eq. [5]) confirms. The relaxation time $(T_2^*)'$ and the diffusion coefficient D, obtained by fitting the first echo amplitude through Eq. [5], are (0.034 ± 0.001) s and $(2.30 \pm 0.08)10^{-9}$ m^2/s, respectively.

The process to follow in order to explain the discrepancies observed between the homogeneous and the heterogeneous

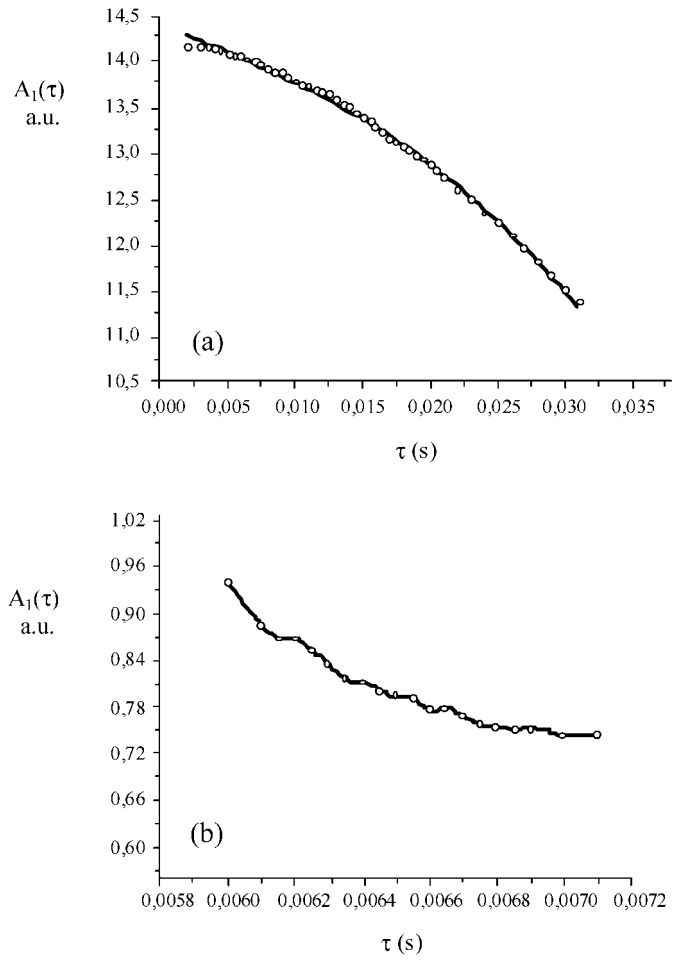

FIG. 5. First echo amplitudes for the sample with 0.5-mm radius beads. In (a) and (b) first echo acquisition is in the same time region of Figs. 3b and 3c, respectively. Averages = 64, $G = 19.7$ mT/m applied along the $\hat{x}$ direction.

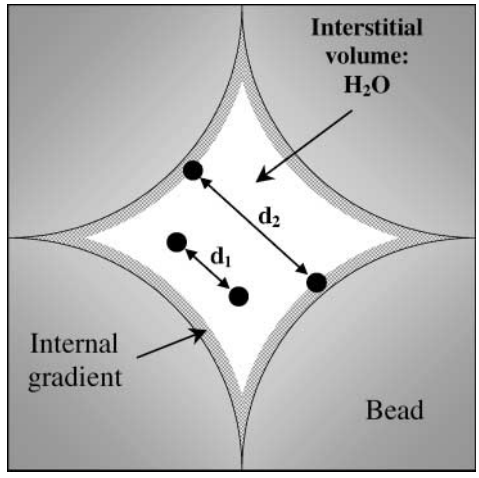

FIG. 6. The spins (black dots), which find themselves at a distance d_1 do not undergo any internal gradients (represented by the checked region). The spins at distance d_2 are instead interacting with internal gradients and their relative phase induced by the external gradient is destroyed.

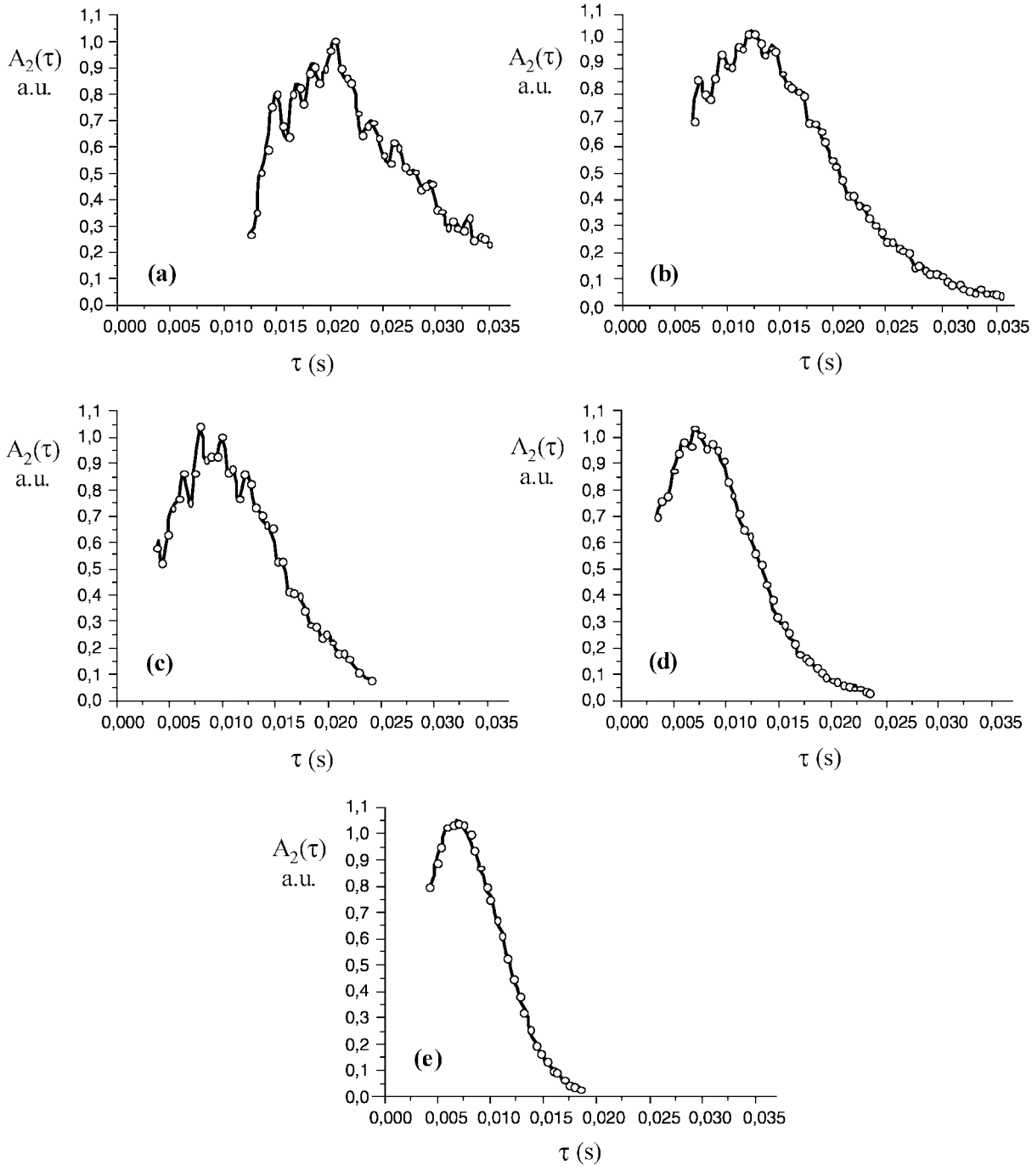

FIG. 7. Collection of second echo curves obtained by varying the external gradient intensity G: (a) $G = 9.8$ mT/m, (b) $G = 14.8$ mT/m, (c) $G = 19.8$ mT/m, (d) $G = 24.8$ mT/m, (e) $G = 29.8$ mT/m. The gradient is always applied along the $\hat{x}$ direction.

samples lies in the particular sensitivity of the second echo amplitude to the local environment. It is well known that strong internal gradients arise when particularly sharp susceptibility differences are present in porous media (18–20) and these highly nonlinear internal gradients are localized at the solid–liquid interface.

In Table 1 a collection of spin–spin relaxation time values obtained with two different techniques for different samples is reported: the standard CPMG sequence and the MSE sequence. For a single sample the spin–spin relaxation values show a substantial difference, which becomes smaller by increasing the pores dimension, namely by increasing the beads radius. Finally

TABLE 1

Comparison between the Spin–Spin Relaxation Values Measured with the CPMG (T_2) and the MSE ($T_2^*)'$ Sequence, Obtained from the Samples Realized with Glass Beads and from the Free Water Sample

	$R = 0.5$ mm	$R = 1$ mm	Free H_2O
$(T_2^*)'$	(0.034 ± 0.001) s	(0.54 ± 0.02) s	(1.52 ± 0.01) s
T_2	(0.230 ± 0.005) s	(0.610 ± 0.01) s	(1.47 ± 0.04) s

for the free water sample this difference becomes negligible. The spin–spin relaxation time behavior confirms the strong dependence of the MSE sequence on the field inhomogeneities, whose effects are instead refocused by the CPMG second pulse (180°).

The question now is how can internal gradient affect the second echo amplitude and cause the observed dips?

In Fig. 6 two different situations are described. The first one represents two spins (black dots) whose distance d_1 is short enough so that they cannot experience the internal gradients, which are strong only near the solid–liquid interface. These spins behave as if they were in a homogeneous system. Their relative phase is just that one imposed by the external gradient. The second situation describes the interaction between two spins whose distance d_2 is comparable with the pore linear dimension. These spins, instead, are affected by the internal gradients. In this last case the coherence between spins, due to the external gradient, is destroyed from the nonlinearity of the internal gradients, and part of the acquired signal is lost. Let us recall that the signal, acquired on the second echo amplitude, comes primarily from those spins, which interact at distances comparable to the correlation distance d. This means that a big part of the acquired signal is lost and the dips appear.

To corroborate this qualitative explanation we compared the results obtained either by varying the external gradient intensity or by varying the pore dimension, namely by changing the beads radius.

In Fig. 7 different MSE experiments are reported for different external gradient intensities G, which are always applied along the $\hat{x}$ direction. By increasing the external gradient, namely by decreasing the correlation distance d, the second echo amplitude behavior slightly approaches the homogeneous curve. The total absence of dips in the last plot obtained for the smallest correlation distance ($G = 29.8$ mT/m) confirms the strict relation between the pore size and the dips. Actually, under these conditions, the interacting spins "see" the porous system as homogeneous.

CONCLUSIONS

The comparison between the measurements obtained for bone samples, travertine samples, and phantoms made of glass beads show the sensitivity of the MSE technique to microstructure in porous media. In particular the strict relation, which occurs between the characteristic length d and the pore dimensions, is evident for all samples.

The great importance of the results presented in this paper lies in the consistent explanation given to the physical origin of the observed dips, based on the role of the internal gradients. The comparison of the second echo curves obtained by varying the correlation distance d (by acting on the external gradient intensity) shows that when the correlation distance d becomes smaller than the pore dimensions, the spins are not subject to internal gradients (namely to the pore walls) and the second echo amplitude behavior approaches that of a homogeneous system. On the other hand, when the correlation distance d approaches the average pore size, the second echo curves show a drop in the signal intensity.

Finally, the MSE technique offers a unique tool to investigate porous structure. As a matter of fact its sensitivity to local susceptibility differences and the possibility of selectively studying heterogeneous systems at different length scales are simply achievable by changing the external gradient intensity and direction. We think that the technique will be widely used in biomedical and materials science applications.

REFERENCES

1. R. Bowtell, R. M. Bowley, and P. Glover, Multiple spin echoes in liquids in a high magnetic field, *J. Magn. Reson.* **88,** 643–651 (1990).
2. R. Bowtell and P. Robyr, Structural investigations with the dipolar demagnetizing field in solution NMR, *Phys. Rev. Lett.* **76,** 4971–4974 (1996).
3. W. S. Warren, W. Richter, A. H. Andreotti, and B. T. Farmer II, Generation of impossible cross-peaks between bulk water and biomolecules in solution NMR, *Science* **262,** 2005–2009 (1993).
4. W. Richter, S. Lee, W. S. Warren, and Q. He, Imaging with intermolecular multiple quantum coherences in solution nuclear magnetic resonance, *Science* **267,** 654–657 (1995).
5. S. Mori, R. E. Hurd, and C. M. van Zijl, Imaging of shifted stimulated echoes and multiple spin echoes, *Magn. Reson. Med.* **37,** 336–340 (1997).
6. W. S. Warren, S. Ahn, M. Mescher, M. Garwood, K. Ugurbil, W. Richter, R. R. Rizi, J. Hopkins, and J. S. Leigh, MR imaging contrast enhancement based on intermolecular zero quantum coherences, *Science* **281,** 247–251 (1998).
7. A. Bifone, G. S. Payne, and M. O. Leach, In vivo multiple spin echoes, *J. Magn. Reson.* **135,** 30–36 (1998).
8. R. R. Rizi, S. Ahn, D. C. Alsop, S. Garrett-Roe, M. Mescher, W. Richter, M. D. Schnall, J. S. Leigh, and W. S. Warren, Intermolecular zero-quantum coherence imaging of the human brain, *Magn. Reson. Med.* **43,** 627–632 (2000).
9. J. Zhong, C. Zhong, and E. Kwok, In vivo intermolecular double-quantum imaging on a clinical 1.5T MR scanner, *Magn. Reson. Med.* **43,** 335–341 (2000).
10. R. Bowtell, Indirect detection via the dipolar demagnetising field, *J. Magn. Reson.* **100,** 1–17 (1992).
11. D. Einzel, G. Eska, and Y. Hirayoshi, Multiple spin echoes in a normal Fermi liquid, *Phys. Rev. Lett.* **53,** 2312–2315 (1984).

12. S. Capuani, F. Curzi, F. M. Alessandri, B. Maraviglia, and A. Bifone, Characterization of trabecular bone by dipolar demagnetizing field MRI, *Magn. Reson. Med.* **46,** 683–689 (2001).

13. S. Capuani, F. M. Alessandri, A. Bifone, and B. Maraviglia, Multiple spin echoes for the evaluation of trabecular bone quality, *MAGMA* **14,** 3–9 (2002).

14. W. J. Whitehouse, Scanning electron micrographs of cancellous bone from the human sternum, *J. Pathol.* **116,** 213–224 (1975).

15. G. Deville, M. Bernier, and J. M. Delrieux, NMR multiple echoes observed in solid ^{3}He, *Phys. Rev. B* **19,** 5666–5688 (1979).

16. S. Capuani, M. Alesiani, F. M. Alessandri, and B. Maraviglia, Characterization of porous media structure by non linear NMR methods, *Magn. Reson. Imag.* **19,** 319–323 (2001).

17. Z. Chen, S. Zheng, Z. Chen, and J. Zhong, Quantitation of transverse relaxation time of intermolecular multiple-quantum coherences, *Proc. Intl. Soc. Mag. Reson. Med.* **9,** 852 (2001).

18. J. Lian, D. S Williams, and I. J. Lowe, Magnetic resonance imaging of diffusion in the presence of background gradients and imaging of background gradients, *J. Magn. Reson. A* **106,** 65–74 (1994).

19. J. A. Hopkins and F. W. Wehrli, Magnetic susceptibility measurement of insoluble solids by NMR: magnetic susceptibility of bone, *Magn. Reson. Med.* **37,** 494–500 (1997).

20. D. J. Bergman, K. J. Dunn, and G. A. LaTorracca, Magnetic field nonuniformities and NMR of protons diffusing in a porous medium, *Magn. Reson. Imag.* **14,** 853–855 (1996).